Nanoscale

PAPER

View Article Online
View Journal | View Issue

Cite this: *Nanoscale*, 2017, **9**, 17387

Attomolar detection of extracellular microRNAs released from living prostate cancer cells by a plasmonic nanowire interstice sensor†

Siyeong Yang,‡[a] Hongki Kim,‡[a] Kyung Jin Lee,[a] Seul Gee Hwang,[b,c] Eun-Kyung Lim,[b,c,d] Juyeon Jung,[b,c] Tae Jae Lee,[e] Hee-Sung Park,*[a] Taejoon Kang *[b,c,d] and Bongsoo Kim *[a]

Prostate cancer (PC) is the second leading cause of cancer death for men worldwide. The serum prostate-specific antigen level test has been widely used to screen for PC. This method, however, exhibits a high false-positive rate, leading to over-diagnosis and over-treatment of PC patients. Extracellular microRNAs (miRNAs) recently provided valuable information including the site and the status of the cancers and thus emerged as new biomarkers for several cancers. Among them, miR141 and miR375 are the most pronounced biomarkers for the diagnosis of high-risk PC. Herein, we report an attomolar detection of miR141 and miR375 released from living PC cells by using a plasmonic nanowire interstice (PNI) sensor. This sensor showed a very low detection limit of 100 aM as well as a wide dynamic range from 100 aM to 100 pM for all target miRNAs. In addition, the PNI sensor could discriminate perfectly the diverse single-base mismatches in the miRNAs. More importantly, the PNI sensor successfully detected the extracellular miR141 and miR375 released from living PC cell lines (LNCaP and PC-3), proving the diagnostic ability of the sensor for PC. We anticipate that the present PNI sensor can hold great promise for the precise diagnosis and prognosis of various cancer patients as well as PC patients.

Received 19th June 2017,
Accepted 7th October 2017

DOI: 10.1039/c7nr04386d

rsc.li/nanoscale

Introduction

MicroRNAs (miRNAs) are single-stranded, small, and noncoding RNAs that play important roles as regulators in numerous biological processes.[1,2] Recently, it has been reported that multiple miRNAs are dysregulated in several human cancers, supporting the hypothesis that miRNAs are involved in the initiation and progression of cancers.[3,4] The dysregulated miRNAs can be released into biological fluids *via* various pathways and thus the expression pattern of miRNAs in cancer cells can be mirrored in biological fluids.[5,6] Consequently, extracellular miRNAs released from cancer cells have been considered as promising noninvasive cancer biomarkers.

Prostate cancer (PC) is one of the most common cancers and the second leading cause of cancer death for men worldwide.[7] Although the serum prostate-specific antigen (PSA) level test has been widely used to diagnose PC, the high false-positive rate of this test has limited the accurate diagnosis of PC.[8,9] The US Preventive Services Task Force even recommended that physicians should not routinely perform PC screening based on serum PSA levels.[10] Therefore, it is highly important to develop a novel PC-specific biomarker detection method. In 2008, it was firstly reported that the level of miR141 is upregulated in the serum of metastatic PC compared with healthy controls and benign prostatic hyperplasia patients.[11] Since then, numerous studies have been conducted to investigate miRNA markers for PC in biological fluids and it was known that the extracellular miR141 and miR375 can provide valuable information of the status and location of the PC site.[12,13] Moreover, extracellular miR141 and miR375 have been the most pronounced biomarkers for high-risk PC, including castrate-resistant PC and metastatic PC, which account for approximately 15% of PC diagnoses and have the potential to progress to a lethal phenotype.[14,15] Thus, it is critical to develop a sensor that is capable of detecting extra-

[a]*Department of Chemistry, KAIST, 291 Daehak-ro, Yuseong-gu, Daejeon 34141, Korea. E-mail: bongsoo@kaist.ac.kr, hspark@kaist.ac.kr*
[b]*Hazards Monitoring BioNano Research Center, 125 Gwahak-ro, Yuseong-gu, KRIBB, Daejeon 34141, Korea. E-mail: kangtaejoon@kribb.re.kr*
[c]*Department of Nanobiotechnology, KRIBB School of Biotechnology, UST, 217 Gajeong-ro, Yuseong-gu, Daejeon 34113, Korea*
[d]*BioNano Health Guard Research Center, 125 Gwahak-ro, Yuseong-gu, KRIBB, Daejeon 34141, Korea*
[e]*Nano-bio Application Team, NNFC, 291 Daehak-ro, Yuseong-gu, Daejeon 34141, Korea*

†Electronic supplementary information (ESI) available. See DOI: 10.1039/c7nr04386d

‡These authors contributed equally to this work.

cellular miR141 and miR375 with high sensitivity and specificity. Recently, the optical and electrochemical sensors have been developed for the detection of miR141 in PC cell lysate.[16,17] While these sensors provide high sensitivity for miR141 through signal amplification processes, it is more desirable to detect the extracellular miRNAs released from living PC cells rather than the miRNAs in PC cell lysate for the practical diagnosis of PC patients. Furthermore, the simultaneous detection of miR141 and miR375 might lead the accurate diagnosis of PC patients.

Herein, we report a plasmonic nanowire (NW) interstice (PNI) sensor which can detect the extracellular miR141 and miR375 released from living PC cells into a culture medium. This sensor shows an extremely low detection limit of 100 aM for both miR141 and miR375, and a wide dynamic range from 100 aM to 100 pM, covering the typical concentration range of extracellular miRNAs in the bloodstreams of patients.[18,19] Additionally, the PNI sensor can completely discriminate the single-base mismatches of miR141 and miR375. This excellent sensing capability of the PNI sensor enables the simultaneous detection of miR141 and miR375 released from the living PC cells (LNCaP and PC-3), showing the potential applicability to a novel PC diagnostic method. Since the PNI sensor can be easily modified for capturing the desired target miRNAs, maintaining the superior sensing ability of miRNAs, we expect that the PNI sensor could apply to the diagnosis and prognosis of the several miRNA-related diseases.

Experimental section

Materials

Au powder (99.99%) and sodium dodecyl sulfate (SDS) were purchased from Sigma-Aldrich. All miRNAs, including the target miRNAs and single-base mismatched miRNAs, were purchased from Bioneer (Daejeon, Korea). The thiolated probe locked nucleic acid (LNA) and Cy5-tagged reporter LNA were purchased from Eurogentec (Seraing, Belgium). Sequences of all miRNAs, probe LNA, and reporter LNA used in this research are described in the ESI (Table S1†). Saline sodium citrate (SSC) buffer solution and ultrapure water were purchased from Biosesang (Sungnam, Korea). The miRNeasy serum/plasma kit was purchased from Qiagen (Germany).

Instrumentation

The surface-enhanced Raman scattering (SERS) spectra were measured using a custom-built micro-Raman system on an Olympus BX41 microscope. A 633 nm He/Ne laser (Melles Griot) was used as an excitation source, and the laser was focused on the PNI sensor through a 100× objective (numerical aperture = 0.7, Mitutoyo). The polarization of the laser was directed by rotating a half-wave plate. The SERS signals were recorded with a thermodynamically cooled electron-multiplying charge-coupled device (Andor) mounted on a spectrometer with a 1200 groove per mm grating (Dongwoo Optron). The acquisition time for all SERS spectra was 100 s. Two holographic notch filters were used to remove the 633 nm light. The cell media were centrifuged using a Microfuge 22R centrifuge (Beckman Coulter). A field-emission scanning electron microscope (FE-SEM, Nova230) was used to obtain SEM images. A field-emission transmission electron microscope (FE-TEM, Tecnai F30 ST) was used to obtain TEM images, high-resolution TEM (HRTEM) images, selected area electron diffraction (SAED) patterns, and fast Fourier transform (FFT) patterns.

Preparation of the PNI sensor

Using the chemical vapor transport method described in a previous report, single-crystalline Au NWs were synthesized on a sapphire substrate in a horizontal quartz tube furnace system.[20] Au powder in an alumina boat was placed in the centre of the heating zone. The sapphire substrate was positioned a few centimeters downstream from the Au powder. The source temperature was increased to 1100 °C while the chamber pressure was maintained at 5–10 Torr. Ar gas flowed at a rate of 100 standard cubic centimeters per minute to transport the Au vapor. The Au NWs were grown on the substrate for a reaction time of 1 h. The single-crystalline Au NWs have a rhombic cross-section, an atomically smooth surface with a diameter of about 200 nm, and a length of several tens of micrometers (Fig. S1 in the ESI†). To modify the surface of the Au NWs with the capture-probe LNA, the as-synthesized Au NWs were incubated in a solution of 10 nM probe LNA, 3× SSC, and 0.04% SDS for 12 h at room temperature. The excessive LNA was rinsed with a solution of 2× SSC and 0.1% SDS. The probe LNA-modified Au NWs were transferred on Au films. The Au films were prepared on Si substrates after electron beam-assisted deposition of a 10 nm-thick film of Cr followed by a 300 nm-thick film of Au. The Au NWs were positioned into the desired alignment on the Au films by using a custom-built nanomanipulator.[21]

Cell culture and purification of extracellular miRNAs

The following human cell lines were used and obtained from the ATCC: two human prostate cancer cell lines (PC-3 and LNCaP) and a human cervical cancer cell line (HeLa). The normal prostate cell line (RWPE-1) was a kind gift from Prof. Namhoon Cho at Yonsei University. All cell lines were tested for mycoplasma contamination and cultured at 37 °C under a humidifying atmosphere at 5%. The LNCaP cells and RWPE-1 cells were grown in RPMI-1640 medium supplemented with 10% (v/v) of fetal bovine serum (FBS), penicillin (100 U ml^{-1}), and streptomycin (100 mg ml^{-1}).[22,23] The PC-3 cells were maintained in FK-12 supplemented with 10% (v/v) of FBS, penicillin (100 U ml^{-1}), and streptomycin (100 mg ml^{-1}).[24] The HeLa cells were cultured in DMEM supplemented with 10% (v/v) of FBS, penicillin (100 U ml^{-1}), and streptomycin (100 mg ml^{-1}).[25] The cells were passaged two to three times a week for total RNA extraction, until reaching a confluency of 90%. Next, the media were collected and centrifuged at 14 000*g* for 10 min to discard the remaining cells and cellular debris. Then, the supernatant was filtered using a 0.2 μm pore filter (syringe

filter, GE Healthcare). All of the miRNAs were purified from the collected media using the miRNeasy serum/plasma kit (Qiagen) according to the manufacturer's protocol. The final purified solution containing extracellular miRNAs (10 μl) was diluted to 200 μl of 5× SSC.

Detection of extracellular miRNAs by the PNI sensor

The PNI sensor was incubated with the extracellular miRNAs in a 5× SSC buffer solution at 42 °C using a rotating hybridization incubator (Agilent) for 16 h. After hybridization, the PNI sensors were rinsed with a pre-warmed solution of 2× SSC buffer solution containing 0.1% of SDS at 42 °C to remove non-bonded miRNAs. Next, the sensor was immersed in a mixture solution of reporter LNAs (10 nM) at 64 °C for 1 h. Finally, the PNI sensor was rinsed with a 2× SSC buffer solution containing 0.1% of SDS and ultrapure water, dried with blowing N_2, and measured using the micro-Raman system.

qRT-PCR assay

The quantitative real-time polymerase chain reaction (qRT-PCR) was performed on a Bio-Rad CFX96 TM real-time system with a GoTaq® 1-step RT-qPCR System (Promega). The samples were incubated in a 96-well plate at 37 °C for 15 min for reverse transcription. Next, the samples were incubated at 95 °C for 10 min and followed by 40 cycles of 95 °C for 10 s, 60 °C for 30 s, and 72 °C for 30 s. The GAPDH gene was used as a control gene and the RWPE-1 cell line was used as a control cell. Primer sequences are as follows: miR141, forward, 5′-CGTCAGATGTCCGAGTAGAGGGGGAACGGCGTAACACTGTC-TGGTAAAGA-3′, reverse, miScript universal primer (Qiagen); miR375, forward, 5′-AGC CGTTTGTTCGTTCGGCT-3′, reverse, miScript universal primer (Qiagen); GAPDH, forward, 5′-ATGGGTGTGAACCATGAGAAG-3′, reverse, 5′-AGTTGTCATG-GATGACCTTGG-3′.

Results and discussion

Principle of extracellular miRNA detection by the PNI sensor

In cancer cells, precursor hairpin miRNAs (pre-miRNAs) are formed in the nucleus and transported into the cytoplasm. The pre-miRNAs are then cleaved by the RNase III, yielding mature miRNA duplexes about 19–23 nucleotides in length. The mature miRNAs can be released from the cancer cells *via* several export mechanisms (Fig. 1a).[6] First, the mature miRNAs are incorporated into exosomes, and these exosomes are released when the multivesicular body that contains the exosomes is fused with the plasma membrane. Second, the miRNAs are released through the microvesicles formed by plasma membrane blebbing. Third, the intracellular miRNAs are released as vesicle-free forms after binding to RNA-binding proteins (argonaute family) or incorporated into high-density lipoproteins (HDLs).[26–29] Because the intracellular miRNAs in the cancer cells can be released into biological fluids *via* the

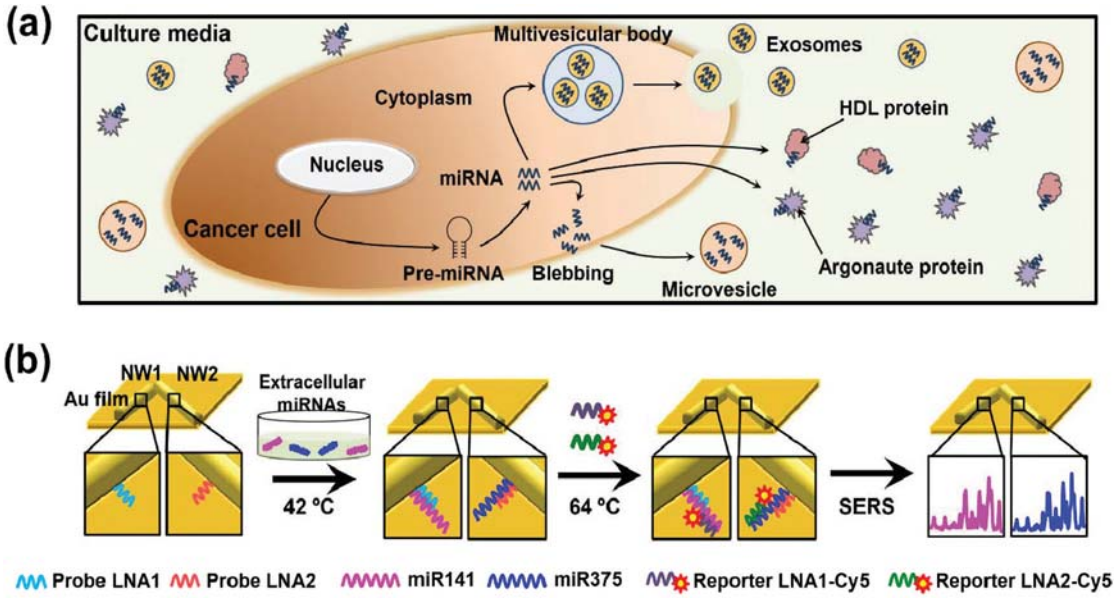

Fig. 1 (a) Representative illustration showing the cellular pathways for miRNA release. In cancer cells, pre-miRNAs are formed in the nucleus and is transported into the cytoplasm. The pre-miRNAs are then cleaved into mature miRNA duplexes. The mature miRNAs can be released from the cancer cells into culture media *via* several export mechanisms. First, the mature miRNAs are incorporated into exosomes, and these exosomes are released when the multivesicular body that contains the exosomes is fused with the plasma membrane. Second, the miRNAs are released through the microvesicles formed by plasma membrane blebbing. Third, the intracellular miRNAs are released as vesicle-free forms after binding to argonaute protein or incorporation into HDL. (b) Schematic illustration of extracellular miRNA detection by using PNI sensors. First, the PNI sensor is prepared by placing Au NW modified with probe LNA onto the Au film. Second, the PNI sensors are incubated at 42 °C with extracellular miRNAs. Third, the PNI sensors are reacted with the Cy5-tagged reporter LNAs at 64 °C. Finally, a complete sandwich structure of probe LNA-miRNA-Cy5-reporter LNA is constructed between the Au NWs and Au film, providing strong SERS signals.

above mechanisms, the expression pattern of miRNAs in cancer cells can be mirrored in biological fluids. This allows the extracellular miRNAs to act as cancer biomarkers. The extracellular miRNAs have strong advantages over protein biomarkers. The miRNAs are stable under harsh conditions such as boiling, pH, and multiple freeze–thaw cycles.[30,31] In addition, the sequences of most miRNAs are conserved among different species.[32] Therefore, identifying the extracellular miRNAs derived from cancer cells is highly desired for the diagnosis of cancers.

To accurately determine the expression patterns of miRNAs in biological fluid samples, it is required to overcome the inconsistent measurement results caused by low specificities and complicated sensing procedures. The optimum miRNA detection method should have (1) highest sensitivity with a wide dynamic range for accurate expression patterns, (2) superb specificity to discriminate the single-base mismatches of miRNAs, and (3) simple processing steps to minimize measurement variation. SERS is a fascinating phenomenon that significantly increases the Raman signal of molecules located within sub 10 nm metallic interstices (hot spots).[33,34] SERS has been employed for the sensitive detection of miRNAs due to its single-molecule sensitivity, molecular specificity, and insensitivity to quenching.[35,36] Previously, our group developed a PNI nanostructure which provides strong, reproducible, and stable SERS signals.[37,38] By combining the PNI nanostructure with the bi-temperature hybridization process, miRNAs could be detected sensitively and selectively.[39,40] We employed a similar sensing strategy with our previous report. Particularly, in this study, we focused on extracellular miR141 and miR375 that are the most pronounced biomarkers for PC. Detection and quantification of extracellular miRNAs present at very low concentrations are quite important for practical diagnosis and prognosis for cancer patients.[11] For the application of the PNI sensor to the diagnosis of PC, we tried to detect miR141 and miR375 simultaneously as depicted in Fig. 1b. In the first step, single-crystalline Au NWs were synthesized in the vapor phase as described in the previous report[20] and the surfaces of Au NWs were modified with probe LNAs through Au–S chemical bonding. LNAs are artificially modified nucleotides with a controlled T_m value, enhancing the affinity for their complementary strands.[41] The probe LNA1 was designed for capturing the miR141 and the probe LNA2 was designed for capturing miR375. The probe LNA1-modified Au NW (NW1) and the probe LNA2-modified Au NW (NW2) were aligned at specific positions on an Au film by using a custom-built nanomanipulator. Because the Au NWs were optically monitored *in situ* while being transferred, the NW1 and NW2 could be clearly distinguishable without additional identification labels. In the second step, the PNI sensors were incubated at 42 °C with extracellular miRNAs. During the incubation, miR141 hybridized with the probe LNA1 of NW1 and miR375 hybridized with the probe LNA2 of NW2, respectively. Next, the PNI sensors hybridized with miR141 and miR375 were immersed in a reporter LNA solution (containing reporter LNA1-Cy5 and reporter LNA2-Cy5) and incubated at 64 °C. This second hybridization process at 64 °C enables the precise discrimination of single-based mismatches of miRNAs (Fig. S2 in the ESI†). After the bi-temperature hybridization process, the perfectly hybridized structure of the probe LNA1-miR141-Cy5-reporter LNA1 remained on NW1 and the structure of the probe LNA2-miR375-Cy5-reporter LNA2 remained on NW2. Finally, we obtained SERS signals from both NW1 and NW2 to identify the presence of miR141 and miR375 in the extracellular miRNAs. Only in the presence of the perfectly matched target miRNAs, PNI sensors could provide strong SERS signals of Cy5. Although miR141 and miR375 were selected as target miRNAs in this study, the PNI sensor could be applied to detect all types of miRNAs by employing the desired probe and reporter LNAs.

Attomolar detection of miRNAs by the PNI sensor

We examined the detection limit and the dynamic range of the PNI sensor for miR141 and miR375, respectively. The optimal miRNA sensor should have low detection limit and a wide dynamic range because the levels of miRNAs released from cancer cells into the circulatory system are very low and vary from person to person. Fig. 2a shows the SERS spectra of Cy5 obtained from the PNI sensor by varying the concentration of miR141. The miR141 samples were prepared using serial dilutions, and a blank sample solution was prepared as a control. The SERS signals of Cy5 gradually decreased as the concentration of miR141 decreased. Notably, the SERS signals were still distinguishable at 100 aM from the signals of blank solution. Fig. 2b also shows the SERS spectra of Cy5 measured from the PNI sensor by varying the concentration of miR375. Similar to the miR141 result, the SERS signals decreased with decreasing the concentration of miR375 and the signals were visible at the low concentration of 100 aM. This suggests that the PNI sensor can detect miR141 and miR375 at the low concentration of 100 aM, corresponding to 50 zeptomoles in a 500 μl volume. Fig. 2c displays the intensity of the Cy5 1580 cm^{-1} band plotted as a function of the miR141 (magenta) and miR375 (blue) concentrations. Both intensities were quite linearly increased throughout the concentration range from 100 aM to 100 pM in spite of the different sequences of miR141 and miR375. We further confirmed the dynamic range of PNI sensors by obtaining the linearly fitted lines of 1580 cm^{-1} band intensity *versus* the concentration of miR141 (magenta) and miR375 (blue) (Fig. 2d). The fitted lines were determined to be $y = 1646.6x + 27\,622.8$ with an R^2 value of 0.99585 for miR141, and $y = 1699.1x + 28\,743.0$ with an R^2 value of 0.99482 for miR375 (x = log concentration). Additionally, we performed a spike-in experiment using Cel-miR-39. Similar to the miR141 and miR375 results, the SERS intensity proportionally increased within the Cel-miR-39 concentration range of 100 aM to 100 pM (Fig. S3a in the ESI†). Moreover, the PNI sensor could detect Cel-miR-39 in human serum (Fig. S3b in the ESI†). Consequently, we tried to detect miR141 and miR375 in human serum by using the PNI sensor. The samples were prepared by spiking miR141 and miR375 into human serum, respectively, and the control was a pure

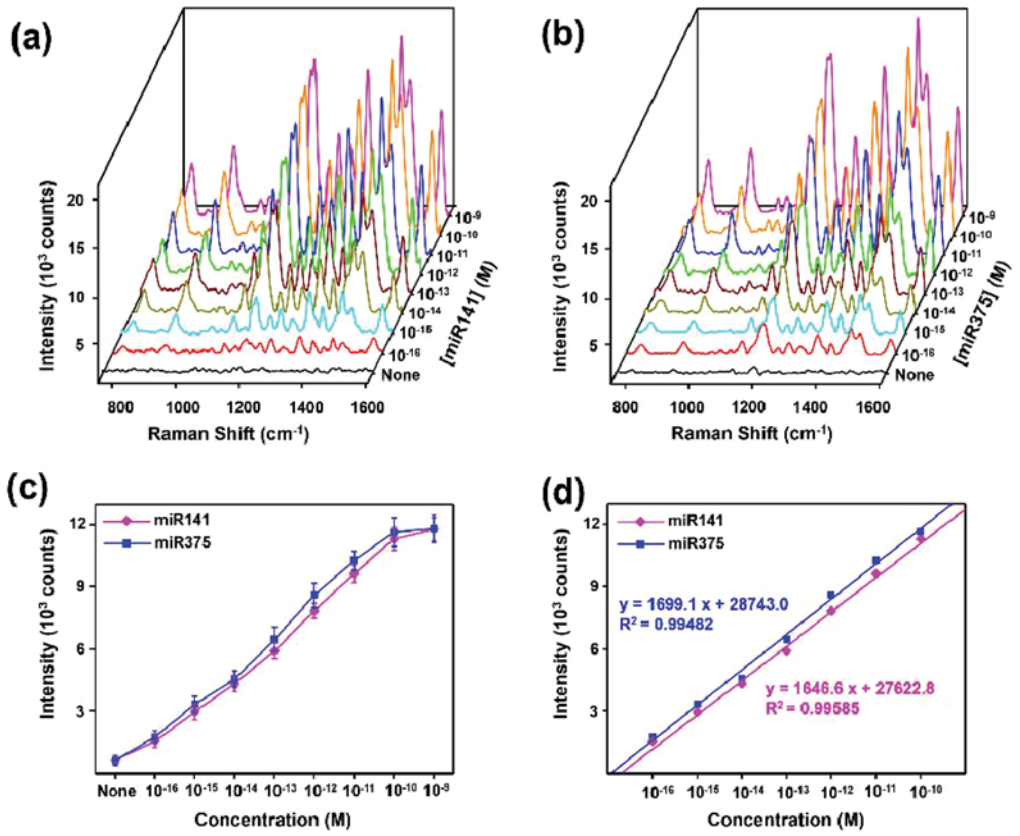

Fig. 2 (a) SERS spectra of Cy5 measured from PNI sensors by varying the concentration of miR141 from 0 M to 1 nM. (b) SERS spectra of Cy5 measured from PNI sensors by varying the concentration of miR375 from 0 M to 1 nM. (c) Plots of 1580 cm^{-1} band intensity *versus* the concentrations of miR141 and miR375. The data represent the mean plus and minus standard deviation from ten measurements. (d) Linearly fitted lines of 1580 cm^{-1} band intensity *versus* the concentrations of miR141 and miR375 (x = log concentration).

human serum. The total RNAs were purified by employing a miRNeasy serum/plasma kit and the purified miRNAs were applied to the PNI sensors. Fig. S4† shows the intensity of the 1580 cm^{-1} band plotted as a function of the spiked miR141 and miR375 concentrations. The SERS intensities almost linearly increased from 100 fM to 1 nM as the spiked concentration of miRNAs increased. This demonstrates that the present method can detect miRNAs even in human serum. The well-defined PNI nanostructure which provides a highly reproducible SERS hot spot line, straightforward probe LNA immobilization, and simple miRNA–LNA hybrid formation with equalized stabilities seems to collectively contribute to the observed equally enhanced and highly reproducible SERS signals for miR141 and miR375.

Perfect discrimination of single-base mismatches in miRNAs by the PNI sensor

Currently, more than 24 000 miRNAs have been identified and they often have similar sequences.[42] In addition, the members of a specific miRNA family usually differ only by a single base in a sequence, because miRNAs that differ by a single-base sequence have different biological roles during the occurrence, inhibition, and metastasis of cancers.[43–45] The optimal miRNA sensor should exhibit a complete specificity that can detect the miRNA with an intact sequence. To investigate the specificity of a PNI sensor, we prepared four kinds of single-base mismatched miRNAs (miR141 A, miR141 B, miR375 A, and miR375 B). The miR141 A and miR375 A had a mismatched single base on the probe LNA recognition site, respectively, and the miR141 B and miR375 B had a mismatched single base on the reporter LNA recognition site. All nucleotide sequences are shown in the inset of Fig. 3. The mismatched bases in miR141 A, B and miR375 A, B are marked in red. The LNA sequences in the probe LNA1, 2 and reporter LNA1, 2 are marked in blue. Fig. 3 shows the plot of Cy5 1580 cm^{-1} band intensity obtained from the PNI sensors for perfectly matched and single-base mismatched miRNAs. The concentration of all miRNAs was 100 pM. When the single-base mismatched miRNAs (miR141 A, B and miR375 A, B) were present, featureless SERS signals were obtained from the PNI sensors. In contrast, significantly strong SERS signals were measured from the PNI sensors in the presence of miR141 and miR375 with intact sequences. In the miRNA sensing procedure using the PNI sensor, the unstable single-base mismatched miRNA–LNA hybridized structures were destroyed at the temperature over T_m. Therefore, we near-perfectly excluded the possibility of detecting single-base mismatched miRNAs. Meanwhile, the SERS signals of miR375 A and B were slightly stronger than

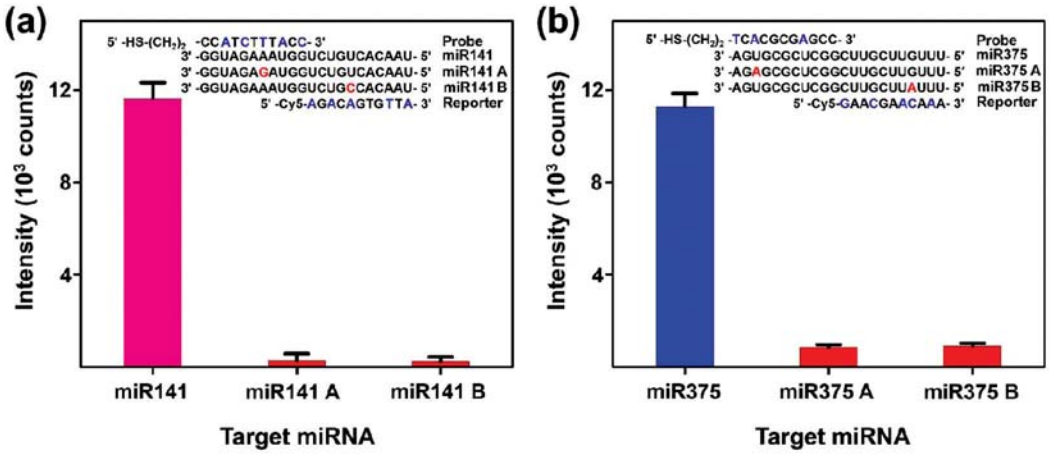

Fig. 3 (a and b) Plots of 1580 cm^{-1} band intensity with various target miRNAs. When the perfectly matched miRNAs (miR141 and miR375) were present, intense SERS signals were obtained from PNI sensors. When the single-base mismatched miRNAs (miR141 A, B and miR375 A, B) were present, indistinctive SERS signals were obtained from PNI sensors. All nucleotide sequences are shown in the inset. LNA sequences and mismatched sequences are annotated with blue and red words, respectively. The data represent the mean plus standard deviation from ten measurements.

those of miR141 A and B. This can be attributed to the fact that the single-base mismatched miR375-LNA hybridized structures contain more GC pairs than the single-base mismatched miR141-LNA structures.[46,47] Furthermore, we examined the discriminating ability of the PNI sensor by employing the let-7 miRNA family (let-7a, let-7b, and let-7c) in human serum. Fig. S5† shows the plot of 1580 cm^{-1} band intensity with various let-7 miRNA families. When the sample contains only let-7a, strong SERS signals were observed from the PNI sensor having probe let-7a. When let-7a and let-7b are present in the sample, SERS signals were obtained from the PNI sensors having probes let-7a and let-7b. When the sample has all three let-7 miRNAs, SERS signals were observed from all PNI sensors. These results clearly show that the PNI sensor can discriminate close miRNA family members in human serum without cross-reactivity. Although various enzymatic detection methods have been developed for identifying single-base mismatches of miRNAs,[48,49] they often suffer from the complexity of optimizing the enzymatic reaction. The present PNI sensor can be prepared in a relatively convenient way, and only produces SERS signals for intact miRNAs. We expect that the PNI sensor would be efficient for the diagnosis of PC and further miRNA-related diseases.

Detection of extracellular miRNAs released from living PC cells by the PNI sensor

Finally, the PNI sensors were employed to detect miR141 and miR375 released from the living PC cells. We prepared four types of media in which different human cancer cell lines were cultured. The cultured cell lines were LNCaP (PC cells), PC-3 (PC cells), RWPE-1 (noncancerous prostate epithelial cells), and HeLa (cervical cancer cells). For the detection of miR141 and miR375 by using PNI sensors, the whole extracellular miRNAs released from the cells into media were isolated and purified by the following procedures (Fig. 4a). First, the cell cultured media were collected. In these collected media, the cells and extracellular miRNAs existed together. Second, the cells and cell debris were discarded by centrifugation and filtration. The centrifugation was performed at 14 000*g* for 10 min, and the supernatant was subsequently filtered using 0.2 μm pore filters. This process enabled the complete removal of the cells and debris from the media.[6,50] After centrifugation and filtration, the extracellular miRNAs were remained in the cell-free media. The extracellular miRNAs, however, were present as complexed forms with argonaute proteins, HDL proteins, exosomes, or microvesicles in the cell-free media. In order to acquire the purified extracellular miRNAs, we performed the purification process using a miRNeasy serum/plasma kit according to the manufacturer's protocol. Lastly, the purified miRNAs were detected using the PNI sensors. The optical image shows the PNI sensors which we obtained as SERS signals. The NW1 and NW2 were designed to provide the SERS signals for miR141 and miR375, respectively. We also measured the levels of extracellular miR141 and miR375 in the cell culture supernatant by using qRT-PCR. Fig. 4b and c represent the extracellular miR141 and miR375 levels determined by the PNI sensor and qRT-PCR, respectively, for LNCaP, PC-3, RWPE-1, and HeLa. The extracellular miRNA sensing results of the PNI sensor agreed well with the results of qRT-PCR, indicating that the PNI sensor can detect extracellular miRNAs released from living PC cells accurately. In both the PNI sensor and qRT-PCR analyses, the levels of miR141 and miR375 in LNCaP and PC-3 culture supernatants were higher than those in RWPE-1 and HeLa. Meanwhile, the fold change relative to RWPE-1 also agreed well with previous reports.[51,52]

We estimated the level of extracellular miRNAs present in the cell line supernatant using the linearly fitted lines as shown in Fig. 2c and d. The estimated levels of miR141 were 12 fM for LNCaP, 7.9 fM for PC-3, 0.2 fM for RWPE-1, and 0.3 fM for HeLa. The estimated levels of miR375 were 24 fM for

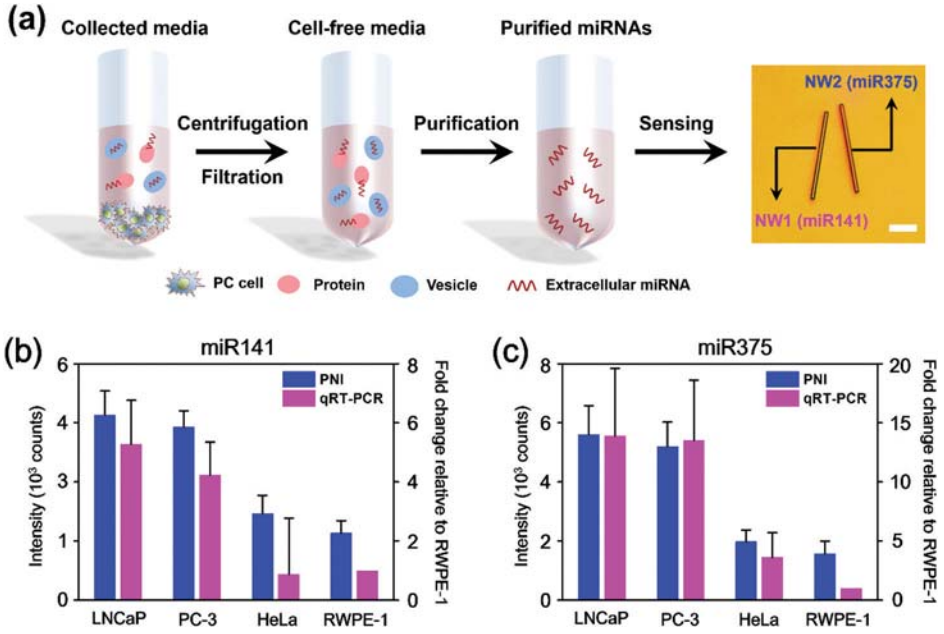

Fig. 4 (a) Schematic illustration of the isolation and purification of extracellular miRNAs released from cancer cells. First, the cancer cell cultured media were collected and the collected media were centrifuged and filtered to discard the cancer cells and cell debris. Next, cell-free media were purified using a miRNeasy serum/plasma kit to obtain the extracellular miRNAs. Lastly, the extracellular miRNAs were detected using the PNI sensors. The optical image shows the PNI sensors which we obtained as SERS signals. The NW1 and NW2 were designed to provide the SERS signal for miR141 and miR375, respectively. The scale bar denotes 500 nm. (b) Extracellular miR141 and (c) miR375 levels determined by the PNI sensor (blue bar) and qRT-PCR (magenta bar) for four kinds of cell culture supernatants (LNCaP, PC-3, RWPE-1, and HeLa). Left axes are the 1580 cm^{-1} band intensities measured from PNI sensors and right axes are the fold change relative to RWPE-1 obtained from qRT-PCR. SERS data represent the mean plus standard deviation from ten measurements. qRT-PCR data represent the mean plus standard deviation from three measurements.

LNCaP, 14.3 fM for PC-3, 0.16 fM for RWPE-1, and 0.18 fM for HeLa. The concentrations of miR141 and miR375 in the LNCaP sample were higher than those in the PC-3 sample, agreeing with the previous reports obtained from cell lysates.[53,54] The PNI sensor can quantitate the extracellular miRNAs unlike other methods that provide relative amounts or indirectly quantifying amounts of miRNAs. The high sensitivity, wide dynamic range, and near-perfect single-base discrimination of the PNI sensor would enable the diagnosis and prognosis of various cancers.

Conclusions

We developed a PNI sensor which can detect extracellular miR141 and miR375 released from living PC cell lines. The proposed PNI sensor exhibited an extremely low detection limit of 100 aM, a wide dynamic range from 100 aM to 100 pM, and a perfect discrimination of single-base mismatches in target miRNAs. By using the PNI sensor, we clearly observed that miR141 and miR375 were released only from living human PC cell lines (LNCaP and PC-3). In addition, we estimated the absolute amount of the released miR141 and miR375 from each PC cell line. The highly sensitive and exactly quantifiable PNI sensor could be useful for the precise diagnosis of PC patients and will be further valuable for detecting other disease-related extracellular miRNAs.

Conflicts of interest

There are no conflicts to declare.

Acknowledgements

This work was supported by the Global Frontier Project (H-GUARD_2014M3A6B2060489 and H-GUARD_2014M3A6B2 060507) through the Center for BioNano Health-Guard funded by the Ministry of Science and ICT (MSIT), Public Welfare & Safety Research Program (NRF-2012M3A2A1051682 and NRF-2013M3A2A107399) through the National Research Foundation (NRF) of Korea funded by MSIT, NRF grant (2017R1A2B4010073) funded by MSIT, and the KRIBB initiative Research Program.

Notes and references

1 E. Kim, J. Yang, J. Park, S. Kim, N. H. Kim, J. I. Yook, J.-S. Suh, S. Haam and Y.-M. Huh, *ACS Nano*, 2012, **6**, 8525–8535.
2 M. Zouari, S. Campuzano, J. Pingarrón and N. Raouafi, *Biosens. Bioelectron.*, 2017, **91**, 40–45.
3 W. Wu, C. Lee, C. Cho, D. Fan, K. Wu, J. Yu and J. Sung, *Oncogene*, 2010, **29**, 5761–5771.

4 J. Lu, G. Getz, E. A. Miska, E. Alvarez-Saavedra, J. Lamb, D. Peck, A. Sweet-Cordero, B. L. Ebert, R. H. Mak and A. A. Ferrando, *Nature*, 2005, **435**, 834–838.
5 N. Kosaka, H. Iguchi and T. Ochiya, *Cancer Sci.*, 2010, **101**, 2087–2092.
6 H. Schwarzenbach, N. Nishida, G. A. Calin and K. Pantel, *Nat. Rev. Clin. Oncol.*, 2014, **11**, 145–156.
7 R. L. Siegel, K. D. Miller and A. Jemal, *CA-Cancer J. Clin.*, 2016, **66**, 7–30.
8 A. Sita-Lumsden, D. A. Dart, J. Waxman and C. Bevan, *Br. J. Cancer*, 2013, **108**, 1925–1930.
9 Z. H. Chen, G. L. Zhang, H. R. Li, J. D. Luo, Z. X. Li, G. M. Chen and J. Yang, *Prostate*, 2012, **72**, 1443–1452.
10 V. A. Moyer, *Ann. Intern. Med.*, 2012, **157**, 120–134.
11 P. S. Mitchell, R. K. Parkin, E. M. Kroh, B. R. Fritz, S. K. Wyman, E. L. Pogosova-Agadjanyan, A. Peterson, J. Noteboom, K. C. O'Briant and A. Allen, *Proc. Natl. Acad. Sci. U. S. A.*, 2008, **105**, 10513–10518.
12 I. Giusti and V. Dolo, *BioMed Res. Int.*, 2014, **2014**, 561571.
13 X. Huang, M. Liang, R. Dittmar and L. Wang, *Int. J. Mol. Sci.*, 2013, **14**, 14785–14799.
14 J. C. Brase, M. Johannes, T. Schlomm, M. Fälth, A. Haese, T. Steuber, T. Beissbarth, R. Kuner and H. Sültmann, *Int. J. Cancer*, 2011, **128**, 608–616.
15 P. J. Bastian, S. A. Boorjian, A. Bossi, A. Briganti, A. Heidenreich, S. J. Freedland, F. Montorsi, M. Roach, F. Schröder and H. Van Poppel, *Eur. Urol.*, 2012, **61**, 1096–1106.
16 C. Yang, B. Dou, K. Shi, Y. Chai, Y. Xiang and R. Yuan, *Anal. Chem.*, 2014, **86**, 11913–11918.
17 X.-P. Wang, B.-C. Yin, P. Wang and B.-C. Ye, *Biosens. Bioelectron.*, 2013, **42**, 131–135.
18 M. Labib, S. M. Ghobadloo, N. Khan, D. M. Kolpashchikov and M. V. Berezovski, *Anal. Chem.*, 2013, **85**, 9422–9427.
19 S. Campuzano, M. Pedrero and J. M. Pingarrón, *Anal. Bioanal. Chem.*, 2014, **406**, 27–33.
20 Y. Yoo, K. Seo, S. Han, K. S. Varadwaj, H. Y. Kim, J. H. Ryu, H. M. Lee, J. P. Ahn, H. Ihee and B. Kim, *Nano Lett.*, 2010, **10**, 432–438.
21 T. Kang, S. M. Yoo, I. Yoon, S. Y. Lee and B. Kim, *Nano Lett.*, 2010, **10**, 1189–1193.
22 E. H. Nunlist, I. Dozmorov, Y. Tang, R. Cowan, M. Centola and H.-K. Lin, *J. Steroid Biochem. Mol. Biol.*, 2004, **91**, 157–170.
23 Y. Cha, J. Lee, H. Han, B. Kim, S. Kang, Y. Choi and N. Cho, *Prostate*, 2016, **76**, 937–947.
24 M. W. Roomi, V. Ivanov, T. Kalinovsky, A. Niedzwiecki and M. Rath, *In Vivo*, 2005, **19**, 179–183.
25 J. Kwon, S.-R. Lee, K.-S. Yang, Y. Ahn, Y. J. Kim, E. R. Stadtman and S. G. Rhee, *Proc. Natl. Acad. Sci. U. S. A.*, 2004, **101**, 16419–16424.
26 G. K. Joshi, S. Deitz-McElyea, T. Liyanage, K. Lawrence, S. Mali, R. Sardar and M. Korc, *ACS Nano*, 2015, **9**, 11075.
27 J. D. Arroyo, J. R. Chevillet, E. M. Kroh, I. K. Ruf, C. C. Pritchard, D. F. Gibson, P. S. Mitchell, C. F. Bennett, E. L. Pogosova-Agadjanyan and D. L. Stirewalt, *Proc. Natl. Acad. Sci. U. S. A.*, 2011, **108**, 5003–5008.
28 D. D. Taylor and C. Gercel-Taylor, *Gynecol. Oncol.*, 2008, **110**, 13–21.
29 A. Turchinovich, L. Weiz and B. Burwinkel, *Trends Biochem. Sci.*, 2012, **37**, 460–465.
30 J. C. Brase, D. Wuttig, R. Kuner and H. Sültmann, *Mol. Cancer*, 2010, **9**, 306.
31 X. Chen, Y. Ba, L. Ma, X. Cai, Y. Yin, K. Wang, J. Guo, Y. Zhang, J. Chen and X. Guo, *Cell Res.*, 2008, **18**, 997–1006.
32 P. Landgraf, M. Rusu, R. Sheridan, A. Sewer, N. Iovino, A. Aravin, S. Pfeffer, A. Rice, A. O. Kamphorst and M. Landthaler, *Cell*, 2007, **129**, 1401–1414.
33 Y. Shen, X. Cheng, G. Li, Q. Zhu, Z. Chi, J. Wang and C. Jin, *Nanoscale Horiz.*, 2016, **1**, 290–297.
34 S. Choi, J. Hwang, S. Lee, D. W. Lim, H. Joo and J. Choo, *Sens. Actuators, B*, 2017, **240**, 358–364.
35 L. Tong, H. Wei, S. Zhang and H. Xu, *Sensors*, 2014, **14**, 7959–7973.
36 J. Docherty, S. Mabbott, W. E. Smith, J. Reglinski, K. Faulds, C. Davidson and D. Graham, *Analyst*, 2015, **140**, 6538–6543.
37 R. Gwak, H. Kim, S. M. Yoo, S. Y. Lee, G.-J. Lee, M.-K. Lee, C.-K. Rhee, T. Kang and B. Kim, *Sci. Rep.*, 2016, **6**, 19646.
38 I. Yoon, T. Kang, W. Choi, J. Kim, Y. Yoo, S.-W. Joo, Q.-H. Park, H. Ihee and B. Kim, *J. Am. Chem. Soc.*, 2008, **131**, 758–762.
39 T. Kang, H. Kim, J. M. Lee, H. Lee, Y. S. Choi, G. Kang, M. K. Seo, B. H. Chung, Y. Jung and B. Kim, *Small*, 2014, **10**, 4200–4206.
40 M. Lee and Y. Jung, *Angew. Chem., Int. Ed.*, 2011, **50**, 12487–12490.
41 B. Vester and J. Wengel, *Biochemistry*, 2004, **43**, 13233–13241.
42 A. Kozomara and S. Griffiths-Jones, *Nucleic Acids Res.*, 2014, **42**, D68–D73.
43 Z. Yu, Z. Li, N. Jolicoeur, L. Zhang, Y. Fortin, E. Wang, M. Wu and S.-H. Shen, *Nucleic Acids Res.*, 2007, **35**, 4535–4541.
44 M. S. Nicoloso, H. Sun, R. Spizzo, H. Kim, P. Wickramasinghe, M. Shimizu, S. E. Wojcik, J. Ferdin, T. Kunej and L. Xiao, *Cancer Res.*, 2010, **70**, 2789–2798.
45 S. Shin, B. Y. Won, C. Jung, S. C. Shin, D. Y. Cho, S. S. Lee and H. G. Park, *Chem. Commun.*, 2011, **47**, 6611–6613.
46 J. D. Pettigrew and J. A. Kirsch, *Philos. Trans. R. Soc. London, Ser. B*, 1998, **353**, 369–379.
47 W. A. Rees, T. D. Yager, J. Korte and P. H. Von Hippel, *Biochemistry*, 1993, **32**, 137–137.
48 Q. Xu, K. Chang, W. Lu, W. Chen, Y. Ding, S. Jia, K. Zhang, F. Li, J. Shi and L. Cao, *Biosens. Bioelectron.*, 2012, **33**, 274–278.
49 X. Wang, X. Lou, Y. Wang, Q. Guo, Z. Fang, X. Zhong, H. Mao, Q. Jin, L. Wu and H. Zhao, *Biosens. Bioelectron.*, 2010, **25**, 1934–1940.
50 A. Turchinovich, L. Weiz, A. Langheinz and B. Burwinkel, *Nucleic Acids Res.*, 2011, **39**, 7223–7233.

51 J. Xiao, A. Y. Gong, A. N. Eischeid, D. Chen, C. Deng, C. Y. Young and X. M. Chen, *Prostate*, 2012, **72**, 1514–1522.
52 J. M. Pickl, D. Tichy, V. Y. Kuryshev, Y. Tolstov, M. Falkenstein, J. Schüler, D. Reidenbach, A. Hotz-Wagenblatt, G. Kristiansen and W. Roth, *Oncotarget*, 2016, **7**, 59589.
53 S. M. Lynch, K. M. O'neill, M. M. McKenna, C. P. Walsh and D. J. McKenna, *Prostate*, 2016, **76**, 1146–1159.
54 P. Costa-Pinheiro, J. Ramalho-Carvalho, F. Q. Vieira, J. Torres-Ferreira, J. Oliveira, C. S. Gonçalves, B. M. Costa, R. Henrique and C. Jerónimo, *Clin. Epigenet.*, 2015, **7**, 42.